Journal of Materials Chemistry A

Accepted Manuscript

ROYAL SOCIETY OF CHEMISTRY

www.rsc.org/materialsA

Journal of Materials Chemistry A RSCPublishing

ARTICLE

Ab initio study of sodium intercalation into disordered carbon

Cite this: DOI: 10.1039/xoxxoooooox

Ping-chun Tsai[a,b], Sai-Cheong Chung[a,c], Shih-kang Lin[b], and Atsuo Yamada[a,c,*]

Received ooth February 2015,
Accepted ooth February 2015

DOI: 10.1039/xoxxoooooox

www.rsc.org/

Graphite, predominantly chosen anode material for the commercial lithium ion batteries (LIBs), has been reported to have negligible intercalation capacity as a sodium ion battery (NIB) anode. Disordered carbon exhibits high Na intercalation capacity and emerges as leading candidates for NIB applications. However, the mechanism of Na^+ ion insertion into disordered carbon is still controversial. Here, we propose an *ab initio* model for disordered carbon and investigate the intercalation mechanism of Na into the layered domains. Our *ab initio* calculations reveal that larger interlayer distance and the presence of defects can effectively overcome the van der Waals interaction between graphene sheets and help Na intercalation to form NaC_8. The calculation results clarify the mechanism of the Na intercalation and account for the presence of sloping and flat regions of charge-discharge curves in disordered carbon reported in numerous experiments. This reveals a new prospect for helping Na intercalation into graphite.

1. Introduction

Lithium ion batteries (LIBs) dominate energy-storage markets for portable devices and play a crucial role in the development of electric vehicles because of their superior power and energy densities[1-3]. However, concerns regarding the future availability of lithium resources are rising. Sodium ion batteries (NIBs) have been drawing increasing attentions because Na is an earth-abundant element and shares common properties of Li[4-6]. However, Na^+ ion has a larger radius than Li^+ ion (1.02 versus 0.76 Å), which causes many of the superior LIB electrode materials unsuitable for NIBs. In particular, graphite is the widely used anode material for the present commercial LIBs, while it has been reported to have very low capacity <35 mAh g^{-1} when used as a NIB anode[7-9].

Disordered carbon exhibits high Na intercalation capacity and emerges as leading candidates for NIB applications[8, 10-16]. However, the mechanism of Na^+ ion insertion into disordered carbon is still controversial. It is believed that the larger interlayer distance of disordered carbon (0.37-0.38 nm), which is larger than the interlayer distance of graphite (~0.34 nm)[11, 15], helps Na^+ ion intercalation. On the other hand, it was found that many defects present in disordered carbon[10-16]. Recent DFT studies showed that the presence of defects would enhance the alkali (Li and Na) adsorption on pristine graphene (comparable to the outermost layer of graphite)[17-24]. As a result, defects may enhance Na intercalation by the strong bonding energy to overcome the van der Waals energy between graphene sheets. However, no satisfactory theoretical analysis has emerged that clarifies the effects of larger interlayer distance and the present of defects on mechanism of sodium intercalation into disordered carbon. This motivates us to build an *ab initio* model for disordered carbon and investigate the mechanism of Na intercalation into the layered domains.

Firstly, we evaluate the reliability of various semi-empirical corrections[25] and vdW exchange-correlation functionals[26-31] to determine the optimal method for the present study. With the best performing vdW-optPBE functional, the model for the layered domains of disordered carbon was built. The influences of the interlayer distances between graphene layers and the presence of defects on the Na intercalation into the layered domains were systematically investigated. To simplify the complexity of the defects in graphene sheet of disordered carbon, typical point defects, mono-vacancy (MV), di-vacancy (DV), and Stone-Wales (SW) defects[32-34], are considered as the defects in disordered carbon. Through a thorough analysis, the mechanisms for the improved Na intercalation capacity are revealed. Moreover, the calculations results account for the presence of sloping and flat regions of charge-discharge curves in disordered carbon reported in numerous experiments[8, 10-16].

2. Computational methods

The *ab initio* calculations were performed in the density functional theory (DFT) framework as implemented in the Vienna *Ab-initio* Simulation Package (VASP)[35] using generalized gradient approximation (GGA) parameterized by Perdew-Burke and Ernzerhof (PBE)[36], with the vdW-optPBE functional. The projector augmented wave (PAW)[37] method with a plane wave cut off of 400 eV was used. The *k*-point

Table 1 Lattice parameters *a* (Å) and *c* (Å) of graphite and LiC_6 and formation energy (E_f, eV) of LiC_6 [6C(graphite)+Li(s) = LiC_6(s)]

		PBE	D2G	D3G	D3BJ	revPBE	optPBE	optB88	optB86b	DF2	revDF2	exp.
Graphite	*a*	2.47	2.47	2.47	2.47	2.48	**2.47**	2.47	2.47	2.48	2.47	**2.46**[38]
	c	8.68	6.43	6.95	6.74	7.17	**6.88**	6.70	6.62	7.04	6.63	**6.71**[38]
LiC_6	*a*	4.33	4.32	4.32	4.32	4.35	**4.34**	4.33	4.33	4.35	4.32	**4.29**[39]
	c	3.77	3.66	3.66	3.62	3.77	**3.70**	3.66	3.65	3.75	3.64	**3.74**[39]
	E_f	-0.07	-0.70	-0.09	-0.07	-0.07	**-0.15**	-0.21	-0.21	-0.09	-0.22	**-0.14**[40]

meshes for Brillouin zone sampling using 15 × 15 × 5 within the Monkhorst-Pack scheme were constructed for lithium, sodium, graphite and first stage Li- and Na-graphite intercalation compounds. For graphene sheets, the *k*-point meshes are 6 × 6 × 1, 5 × 5 × 1, 4 × 4 × 1, 3 × 3 × 1, 3 × 3 × 1, and 2 × 2 × 1 for the 3 × 3, 4 × 4, 5 × 5, 6 × 6, 7 × 7 and 8 × 8 super cells, respectively. In addition, to avoid the spurious coupling effect between periodic graphene layers along the normal direction, a vacuum separation in the model structure was set to 18 Å. Spin-polarization was included in the calculations. The numerical integration of the Brillouin zone and energy cut-off were reached to produce absolute energy convergence to better than 10^{-4} eV/atom, with the forces at each atom converged to within 10^{-3} eV/Å by the relaxation of internal positions and cell volume.

3. Results and discussion

3.1 Assessment of the employed vdW functionals

The poor description of vdW interactions in conventional exchange-correlation functionals is a fundamental limitation of standard DFT to describe graphite and other carbon layered materials. It is necessary to evaluate the reliability of various vdW functionals to describe the present system. Graphite and Li-graphite are suitable materials for the assessment of vdW functionals because Li-graphite systems have well-known properties and Li share similar properties with Na. We compared the computed results from no vdW correction, three semi-empirical corrections (vdW-D2 vdW-D3, vdW-D3BJ), five vdW functionals (vdW-revPBE, vdW-optPBE, vdW-optB88, vdW-optB86b, vdW-DF2) and the more recent vdW-revDF2[31] functional with the experimental data of graphite and Li-graphite to assess their performance (see Supporting Information, SI).

In graphite, the interlayer distance *c* is perpendicular to the graphene layers and along the direction of the van der Waals interactions. Therefore, the vdW methodologies can be assessed with the aid of the equilibrium interlayer distance *c* of graphite. Figure S1 shows the formation energies of graphite as a function of the interlayer distance *c*, where the minimum binding energy defines the equilibrium interlayer spacing *c*. As shown in Figure S1, GGA, as expected, could not yield a minimum in the binding energy curve of graphite, while all the vdW corrected methods improve the treatment of interlayer interactions by introducing dispersion interactions. The calculated equilibrium lattice parameters (*a* and *c*) of graphite are summarized in Table 1. It is found that the vdW functional-revDF2 gave the best agreement with experimental data in the interlayer distance *c* of graphite[38]. The in-plane lattice parameter *a*, governed by the C-C covalent bonding, does not evidently depend on the employed vdW functionals and the calculated values of PBE also agree well with the experimental value[38].

For the Li-graphite intercalation compound (LiC_6), Li–C interactions dominate over vdW interactions, and the lattice parameters (*a* and *c*) of LiC_6 compound[39] can be well described by the standard GGA as shown in Table 1. However, many key characteristics of lithium ion battery electrode, reversible capacity and voltage, are mainly determined by the strength of binding between Li and the electrode material. The effects of various vdW functionals on the formation energy (binding energy) of LiC_6 must be carefully examined. The calculated formation energies are summarized in Table 1, and the vdW-optPBE functional demonstrates the best agreement with the experimental value[40] while other vdW functionals have noticeable deviations.

For further assessment of the employed vdW functionals, the strength of Li adsorption on graphene (or on the outermost layer of graphite) is examined. Figure S2 shows that the contributions of vdW forces to the adsorption energy of Li on graphene are much dependent on the vdW functionals. Comparing to the PBE functional, the vdW-D3, vdW-D3BJ, vdW-optPBE, vdW-optB88, vdW-optB86b, and vdW-revDF2 functionals are more binding, contributes ~0.1 eV more to the adsorption energy, while the vdW-D2 is significantly (~0.4 eV) more binding. On the other hand, vdW-revPBE and vdW-DF2 are less binding than the PBE functional. It is well known that the interaction between Li and C is governed by charge transfer and therefore ionic bonding, thus, the long-range vdW forces should make little contribution to the adsorption energy. As a result, the vdW-D3, vdW-D3BJ, vdW-optPBE, vdW-optB88, vdW-optB86b, and vdW-revDF2 seem to be more reasonable.

The most reliable vdW functional was decided as a compromise to simultaneously describe the lattice parameter *c* of graphite, the adsorption energies of Li-graphene and more importantly, the formation energy of Li-graphite which greatly dominate the intercalation mechanism in Table 1. As a result, vdW-optPBE was chosen as the most reliable vdW functional as it results in an excellent agreement with the formation energy of LiC_6 and reasonable lattice parameter *a* and *c* of graphite and adsorption energy of the Li-graphene.

3.2 Defects in disordered carbon

The layered regions (layered domains) of disordered carbon is formed by a stack of graphene sheets. To simplify the complexity of the defects in graphene sheet of disordered carbon, typical point defects, mono-vacancy (MV), di-vacancy (DV), and Stone-Wales (SW) defects, are considered because

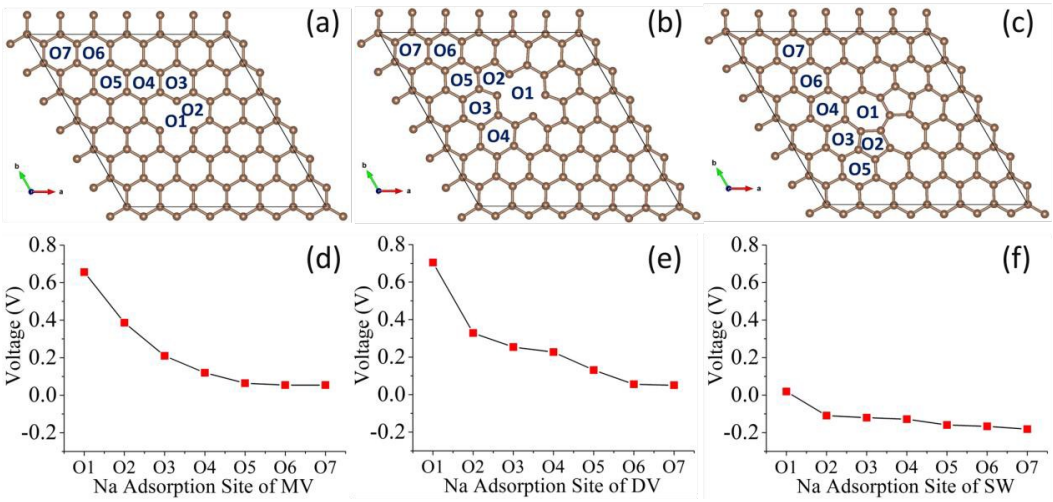

Figure 1 Inequivalent hollow sites O_i (a)-(c) of MV, DV, and SW defective graphene corresponding to the sodiation potential (d)-(f), respectively.

they are commonly seen and dominant in the defective graphene according to TEM and STM observations[32-34]. The 6 × 6 supercell was chosen as the most suitable size to simulate the point defect in graphene sheet, calculated formation energies agree excellently with the experimental values (7.3−7.5 eV for MV, 7.2−7.9 eV for DV, and 4.5−5.3 eV for SW) as shown in Figure S3.

The sodiation potential (V_s) of Na adatom on the defective graphene was calculated as follows:

$$V_s = -(E_{Na-surf} - E_{surf} - E_{Na}) \quad (1)$$

where $E_{Na-surf}$, E_{surf}, and E_{Na} are the total energies of one Na adatom adsorbed on the surface of graphene, the free surface of graphene, and the Na bulk respectively. On pristine graphene, the sodiation potential of Na adatom on the hollow site is −0.31 V, indicating Na adsorption is unstable with respect to Na plating (bulk formation). For the MV, DV, and SW defective graphene, the sodiation potentials on inequivalent hollow sites O_i around the defect zones are presented in Figure 1 (a)-(f). One sees that all the values for MV and DV are positive, while SW values are mainly negative. On the MV defective graphene, the most stable site (the highest sodiation potential) for Na adsorption is the hollow site O_1 (above the center of the MV site) with a voltage of about 0.66 V (Figure 1 (d)). For the other O_i sites, the stability of Na adsorption decreases as the Na adatom gets further away from the MV defect. For the DV case the magnitude is larger but the trend of Na adsorption is similar to the case of the MV defect and is shown in Figure 1 (e). For the SW defect, only the adsorption on the heptagonal ring results in positive voltage. The distances of Na ions above the graphene planes (*d*) and charge transfer to the graphene for the most stable sites in each defect are summarized in Table S1. The larger carbon rings allow Na ions to approach closer to the graphene planes, in case of pristine graphene, *d* is 2.13 Å, whereas for graphene with SW, MV, and DV defects, *d*s decrease to 2.09 Å, 2.08 Å, and 1.90 Å, respectively. This in addition to the larger charge transfer allows stronger ionic interactions for Na with the substrates. As a result, the presence of defects can enhance the Na adsorption on graphene (comparable to the outermost layer of graphite), especially MV and DV defects.

3.3 Na intercalation into disordered carbon

For the pristine graphite, the mechanism of Li and K intercalation into graphite is the stage formation[42], where stage *n* contains *n* empty layers between each Li/K-filled layer. Li/K atoms in stage-I structures of LiC_6 and KC_8 order in ($\sqrt{3} \times \sqrt{3}$) and (2 × 2) manners respectively. However, stage-I structures of NaC_6 and NaC_8 could not be achieved. Their sodiation potentials (V_s) of [Na+C_6→NaC_6] and [Na+C_8→NaC_8] are calculated to be −0.17 V and −0.13 V, respectively, as follows,

$$V_s = -(E_{Na-C} - E_C - E_{Na}) \quad (2)$$

where E_{Na-C}, E_C, and E_{Na} are the total energies of the Na intercalated into graphite, graphene, and the Na bulk. In this study, the (2 × 2) ordering of NaC_8 is assumed as NaC_8 is calculated to be more stable than NaC_6. The staging phenomenon is a thermodynamic behavior related to the energy required to overcome the van der Waals interactions between two graphene layers, guests fill every layer by a stepwise process. To fully understand the thermodynamic behavior of Na intercalation into disordered carbon, we focus the investigation on the mechanism of Na intercalation into empty layer between two graphene sheets, one intercalation layer is gradually filled with Na^+ ions to the (2 × 2) ordering of NaC_8, and a 6 × 6 × 2 graphene model is chosen as the layered regions (layered domains) in disordered carbon.

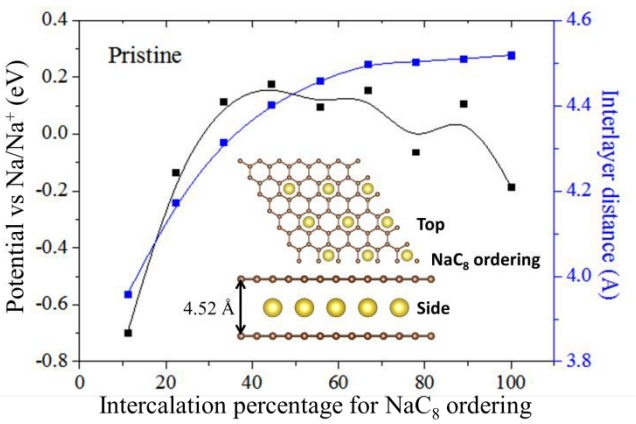

Figure 2 The sodiation potential and interlayer distances of Na^+ ion into one empty intercalation layer formed by the 6 x 6 x 2 pristine graphene model.

For the pristine graphite model, the sodiation potential profile as a function of Na content is presented in Figure 2. The sodiation potential is much negative (-0.7 V) at low Na content, indicates that Na intercalation into graphite is thermodynamically unstable compare to Na plating (at 0 V). However, the sodiation potential keeps rising with the content of Na, flattens off at medium to high Na content, then oscillates about 0 V with a spread of about ±0.1 V. This sodiation potential profile correlates well with the interlayer distance (Figure 2). The reason for the high correlation between sodiation potential and interlayer distance is related to the energy required to overcome the van der Waals interactions between two graphene layers.

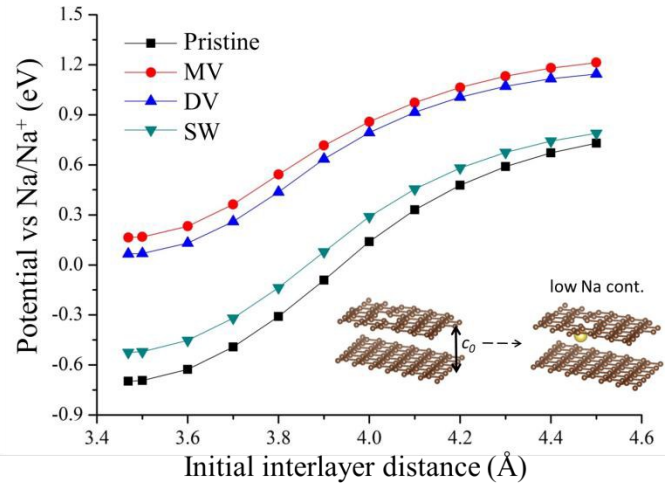

Figure 3 The sodiation potential at low Na content as a function of the initial interlayer distances c_0 for pristine, MV, DV, and SW.

To examine the effect of initial interlayer distance on the Na^+ ion intercalation, the sodiation potential at low Na content as a function of the initial interlayer distance c_0 between two graphene are shown in Figure 3. It can be found that when the initial interlayer distances increase to 3.94 Å, the sodiation potential gradually increase to zero from initial −0.7 V, indicating that intercalation become favorable compare to Na plating when the initial interlayer distances is larger than 3.94 Å. However, the interlayer distance of 3.94 Å is much larger that the experimental observation of 3.7-3.8 Å in most disordered carbon anode materials for NIBs[10-16]. Therefore, the larger interlayer distance is not the only factor to help Na intercalation.

The effects of defects on the Na intercalation into disordered carbon were investigated, a 6 × 6 × 2 model is formed by one pristine and one defective graphene, and MV, DV, or SW point defects are introduced. The first intercalated Na^+ ion is stored near the defect sites due to strong binding energy between Na^+ ion and the defects. The sodiation potentials at low Na content as a function of the initial interlayer distance c_0 for various point defects are shown in Figure 3. For the MV and DV defects, the sodiation potential dramatically increase to positive values and the Na can directly intercalate into disordered carbon without the effect of larger initial interlayer distances. For the SW defect, the sodiation potential increases to less negative value. It is clear that the presence of defects can enhance the Na intercalation, especially the MV and DV defects.

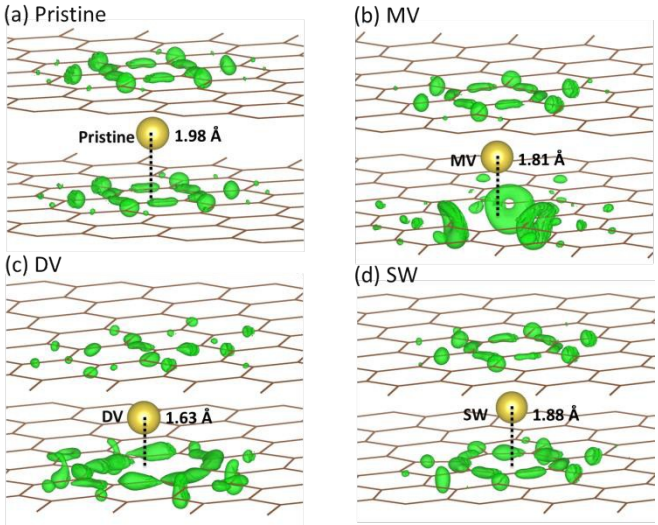

Figure 4 The electronic density differences (only the electron gain is shown) of Na intercalation into one empty layer for (a) pristine, (b) MV, (c) DV, and (d) SW, respectively.

The intercalated Na atoms are fully oxidized in all the models considered, and Table S1 shows the bonding between Na and carbon is ionic in nature. To obtain the insights of the effects of the point defects on the interactions between Na^+ ion and graphene layers, the electronic density analysis were performed. The electronic density difference ($\Delta\rho$) is obtained as the difference between the electronic densities of the Na-graphene layers (ρ_{Na-C}) and those of the graphene layers (ρ_C) and sodium (ρ_{Na}) as follows:

$$\Delta\rho = \rho_{Na-C} - \rho_C - \rho_{Na} \quad (3)$$

Figure 4 (a)-(d) shows the electronic density accumulation (red color). It is found that valence electronic density of the Na atom has transferred almost totally to the bonding carbon rings, confirming the ionic character of the bonding between Na^+ ions and carbons. However, the transferred electronic density tends to accumulate around the defects, as shown in Figure 4 (b)-(d), especially for MV and DV. This effect, in addition to the shorter interplane distances (Table S1) allow stronger ionic binding between Na^+ ion and defective carbon which can conquer the vdW energy to help Na intercalate into the layer between adjacent graphenes.

This analysis also shed some light on the feature of both the sloping and flat regions of charge-discharge curves of disordered carbon anode materials in extensive experimental reports[10-16]. The potential of Na storage in one empty layer of graphite with 3.8 Å interlayer distance (typical in disordered carbons) and one DV defect based on the 6 × 6 × 2 graphene model. The sloping part reflects a strong binding energy that corresponds to the Na adsorption on defective carbon surface and intercalation into disordered carbon, while the plateau region corresponds to the intercalation into sites around the defects. This features agrees well with experimental observation when Na is stored in various disordered carbon materials[8, 10-16]. However, the relatively high Na potential (1.2-1.5 V) in literature finding may be resulting from a strong bond to the surface induced by the presence of oxygen functional groups since it was evident from XPS spectra the presence of functional groups in the various carbon[11, 41, 42].

Conclusions

With *ab initio* calculations using the vdW-optPBE functional, the model for disordered carbon was built and the effects of the initial interlayer distances and defects (MV, DV, and SW) on the Na intercalation into the layered domains were systematically investigated. The *ab initio* model clarifies that large initial interlayer distances and MV, DV, and SW defects favor Na^+ ion intercalation into layered domains. In particular, the vacancy defects (MV and DV) can greatly enhance the Na^+ ion intercalation because of strong ionic binding energy between the Na^+ ion and the defects, which effectively overcome the van der Waals interaction. Moreover, larger interlayer distance and defects may account for both the sloping and flat regions of charge-discharge curves of disordered carbons in experiments. The calculation results clarify the mechanism of the Na intercalation and reveal a new prospect for helping Na intercalation into graphite.

Acknowledgements

This work is supported by the Ministry of Education, Culture, Sports, Science and Technology, Japan (MEXT) under the 'Elemental Strategy Initiative for Catalysts & Batteries' (ESICB) project. P.-C. Tsai and S.-K. Lin thank Professor Masahiro Yoshimura and the financial support from the Interchange Association, Japan and Ministry of Science and Technology, Taiwan (MOST 103-3113-E-024-001).

Notes and references

[a]Department of Chemical System Engineering, The University of Tokyo, 7-3-1 Hongo, Bunkyo-ku, Tokyo 113-8656, Japan. E-mail: yamada@chemsys.t.u-tokyo.ac.jp (A. Yamada), chung@battery.t.u-tokyo.ac.jp (S.-C Chung), and r54iq1000@gmail.com (P.-C Tsai).
[b]Department of Materials Science and Engineering, National Cheng Kung University, Tainan 70101, Taiwan. E-mail: linsk@mail.ncku.edu.tw (S.-K. Lin).
[c]Unit of Element Strategy Initiative for Catalysts & Batteries, ESICB, Kyoto University, Kyoto 615-8510, Japan.

† Electronic Supplementary Information (ESI) available: formation energies of graphite as a function of interlayer distance *c* and adsorption energies of Li as a function of distance from the graphene sheet both calculated by GGA and nine different vdW functionals, defect formation energies of MV, DV, and SW point defects from 3 x 3 to 8 x 8 supercell sizes of graphene, and charge transfer from Na^+ ions to graphene sheet and vertical distances (Å) between Na^+ ion and the graphene sheet for Na adsorption on a graphene sheet and intercalation into layer between graphene sheets.

1. A. Yamada, *MRS Bull.*, 2014, **39**, 423.
2. X.-P. Gao and H.-X. Yang, *Energy Environ. Sci.*, 2010, **3**, 174.
3. B. Scrosati and J. Garche, *J. Power Sources*, 2010, **195**, 2419.
4. P. Barpanda, G. Oyama, S.-i. Nishimura, S.-C. Chung and A. Yamada, *Nat. Commun.*, 2014, **5**, 4358.
5. M. D. Slater, D. Kim, E. Lee and C. S. Johnson, *Adv. Funct. Mater.*, 2013, **23**, 947.
6. N. Yabuuchi, K. Kubota, M. Dahbi and S. Komaba, *Chem. Rev.*, 2014. **114**, 11636.
7. P. Ge and M. Fouletier, *Solid State Ionics*, 1988, **28**, 1172.
8. D. Stevens and J. Dahn, *J. Electrochem. Soc.*, 2001, **148**, A803.
9. Y. Mizutani, T. Abe, M. Inaba and Z. Ogumi, *Synth. Met.*, 2001, **125**, 153.
10. D. Stevens and J. Dahn, *J. Electrochem.*, 2000, **147**, 1271.
11. S. Komaba, W. Murata, T. Ishikawa, N. Yabuuchi, T. Ozeki, T. Nakayama, A. Ogata, K. Gotoh and K. Fujiwara, *Adv. Funct. Mater.*, 2011, **21**, 3859.
12. J. Zhao, L. Zhao, K. Chihara, S. Okada, J.-i. Yamaki, S. Matsumoto, S. Kuze and K. Nakane, *J. Power Sources*, 2013, **244**, 752.
13. A. Ponrouch, A. Goñi and M. R. Palacín, *Electrochem. Commun.*, 2013, **27**, 85.
14. K. Tang, L. Fu, R. J. White, L. Yu, M. M. Titirici, M. Antonietti and J. Maier, *Adv. Energy Mater.*, 2012, **2**, 873.
15. Y. Cao, L. Xiao, M. L. Sushko, W. Wang, B. Schwenzer, J. Xiao, Z. Nie, L. V. Saraf, Z. Yang and J. Liu, *Nano Lett.*, 2012, **12**, 3783.
16. S. Wenzel, T. Hara, J. Janek and P. Adelhelm, *Energy Environ. Sci.*, 2011, **4**, 3342.
17. Y. Liu, V. I. Artyukhov, M. Liu, A. R. Harutyunyan and B. I. Yakobson, *J. Phys. Chem. Lett.*, 2013, **4**, 1737.
18. L.-J. Zhou, Z. Hou and L.-M. Wu, *J. Phys. Chem. C*, 2012, **116**, 21780.
19. R. Mukherjee, A. V. Thomas, D. Datta, E. Singh, J. Li, O. Eksik, V. B. Shenoy and N. Koratkar, *Nat. Commun.*, 2014, **5**, 3710.
20. D. Datta, J. Li and V. B. Shenoy, *ACS Appl. Mater. Interfaces*, 2014, **6**, 1788.
21. L.-J. Zhou, Z. F. Hou, L.-M. Wu and Y.-F. Zhang, *J. Phys. Chem. C*, 2014, **118**, 28055.
22. D. Datta, J. Li, N. Koratkar and V. B. Shenoy, *Carbon*, 2014, **80**, 305.
23. Y. Liu, Y. M. Wang, B. I. Yakobson and B. C. Wood, *Phys. Rev. Lett.*, 2014, **113**, 028304.
24. H. Yildirim, A. Kinaci, Z.-J. Zhao, M. K. Chan and J. P. Greeley, *ACS Appl. Mater. Interfaces*, 2014, **6**, 21141.
25. S. Grimme, J. Antony, S. Ehrlich and H. Krieg, *J. Chem. Phys.*, 2010, **132**, 154104.
26. M. Dion, H. Rydberg, E. Schröder, D. C. Langreth and B. I. Lundqvist, *Phys. Rev. Lett.*, 2004, **92**, 246401.
27. G. Román-Pérez and J. M. Soler, *Phys. Rev. Lett.*, 2009, **103**, 096102.
28. J. Klimeš, D. R. Bowler and A. Michaelides, *J. Phys.: Condens. Matter*, 2010, **22**, 022201.
29. K. Lee, É. D. Murray, L. Kong, B. I. Lundqvist and D. C. Langreth, *Phys. Rev. B*, 2010, **82**, 081101.
30. J. Klimeš, D. R. Bowler and A. Michaelides, *Phys. Rev. B*, **83**, 195131.
31. I. Hamada, *Phys. Rev. B*, 2014, **89**, 121103.
32. J. C. Meyer, C. Kisielowski, R. Erni, M. D. Rossell, M. Crommie and A. Zettl, *Phys. Rev. B*, 2008, **8**, 3582.
33. J. Kotakoski, A. Krasheninnikov, U. Kaiser and J. Meyer, *Phys. Rev. Lett.*, 2011, **106**, 105505.
34. H. Terrones, R. Lv, M. Terrones and M. S. Dresselhaus, *Rep. Prog. Phys.*, 2012, **75**, 062501.
35. G. Kresse and J. Furthmüller, *Phys. Rev. B*, 1996, **54**, 11169.

36. J. P. Perdew, K. Burke and M. Ernzerhof, *Phys. Rev. Lett.*, 1996, **77**, 3865.
37. P. E. Blöchl, *Phys. Rev. B*, 1994, **50**, 17953.
38. P. Trucano and R. Chen, *Nature*, 1975, **258**, 136
39. R. Juza and V. Wehle, Naturwissenschaften, *Phys. Rev. B*, 1965, **52**, 560.
40. M. Dresselhaus and G. Dresselhaus, *Adv. Phys.*, 1981, **30**, 139.
41. J. Gnanaraj, M. Levi, E. Levi, G. Salitra, D. Aurbach, J. E. Fischer and A. Claye, *J. Electrochem. Soc.*, 2001, **148**, A525.
42. D. Aurbach, B. Markovsky, I. Weissman, E. Levi and Y. Ein-Eli, *Electrochim. Acta*, 1999, **45**, 67.

Journal of Materials Chemistry A RSCPublishing

ARTICLE

The table of contents entry

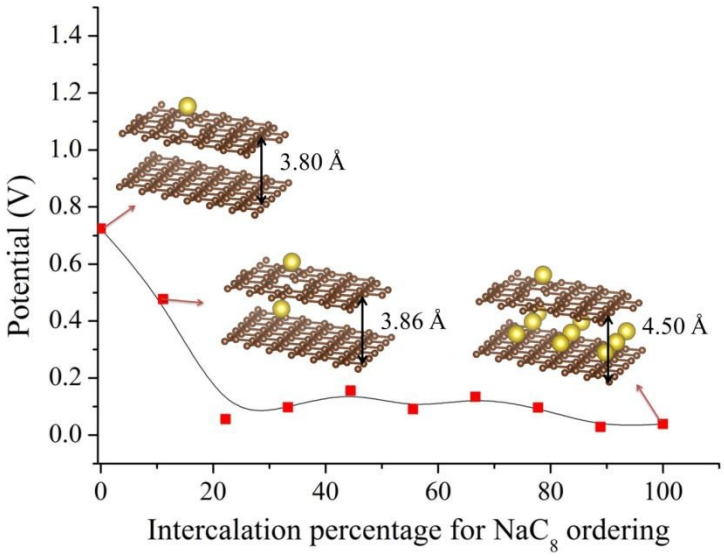

Highlighting the novelty of the work:

Larger interlayer distance and defects may account for both the sloping and flat regions of charge-discharge curves of disordered carbons.